

Aznalcóllar dam failure. Part 1: Field observations and material properties

E. E. ALONSO* and A. GENS*

The paper describes the failure of Aznalcóllar dam, in southern Spain, in April 1998. The rockfill dam slid forward and released a flow of acid-saturated tailings. The geology and geomorphology of the site are described. The results of a detailed laboratory testing programme on the tailings material and on the overconsolidated high-plasticity foundation clay are given. Special attention is paid to the identification of cementation of the tailings and to the strength and consolidation properties of the foundation clay. Failure features are interpreted on the basis of the field evidence, taking into account the measured geotechnical properties of the materials involved.

KEYWORDS: case history; clays; dams; geology; landslides; shear strength

Cet exposé décrit la rupture du barrage d'Aznalcóllar, dans le sud de l'Espagne en avril 1998. Le barrage en enrochements en vrac a glissé en avant, laissant échapper une coulée de déchets résiduels saturés d'acides. Nous décrivons la géologie et la géomorphologie du site. Nous donnons les résultats détaillés d'un programme d'essai en laboratoire sur des déchets résiduels et sur l'argile de fondation fortement plastique et surconsolidée. Nous accordons une attention spéciale à l'identification de la cimentation des déchets résiduels ainsi qu'à la puissance et aux propriétés de consolidation de l'argile de fondation. Nous interprétons les facteurs de défaillance en nous basant sur l'évidence sur le terrain et en prenant en compte les propriétés géotechniques mesurées des matériaux concernés.

INTRODUCTION

The Aznalcóllar tailings dam failed catastrophically in April 1998, causing one of the worst-ever environmental disasters in Spain. The dam was part of a large open-cast mining complex that had been in operation for decades in the vicinity of Aznalcóllar village in the province of Seville, Spain. The mine is located in the pyritic 'mining corridor', well known from ancient times as a productive area for metals such as lead and copper. The most recent activity of the Aznalcóllar mine includes the exploitation of: pyrites (iron disulphides), which is the major component (78–83%) of the mineral extracted; blende or sphalerite (a zinc sulphide); galena (lead sulphide); chalcopyrites (or copper pyrites: copper iron sulphides); and other minerals in minor traces.

Non-exploitable rocks amounted for 85% of the total excavated volume. They included shales, greywackes, dacites, felsites and rhyolites. Consequently, large quantities of excavated rock were available in the mine for auxiliary works and in particular for the construction of the perimeter embankment of the tailings disposal lagoon.

The location of the mine, together with a satellite image of the mining quarries and the disposal lagoon, is shown in Fig. 1. The mine is located in the northern part of the Guadalquivir basin, the elongated triangular shape of which can easily be identified in the map. This basin was an open sea in Miocene times, and was filled by thick deposits of carbonate high-plasticity clays (known often as 'Guadalquivir blue marls' or 'Guadalquivir blue clays'). The tailings lagoon, which has an irregular hexagonal shape in plan view, was founded on a deposit of marine clays having a thickness of no less than 60 m in the centre of the lagoon. A small river (the Agrio river: *agrio* means sour, acidic, acid), which rises on nearby higher ground, where the mine

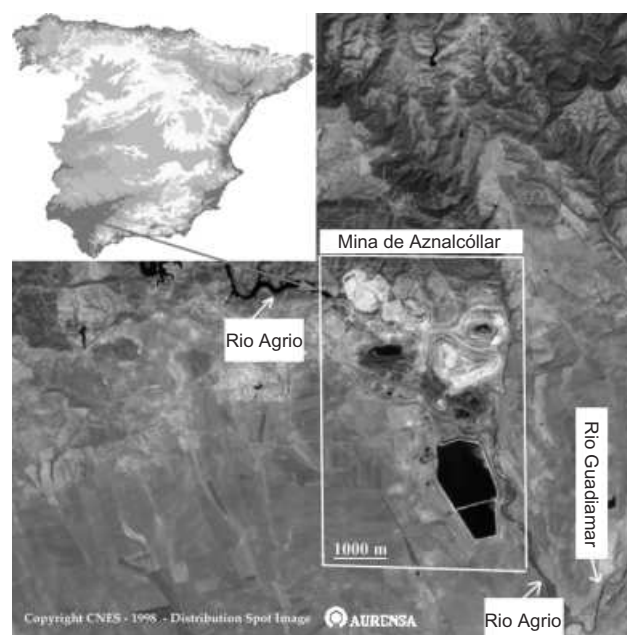


Fig. 1. Location of Aznalcóllar tailings deposit

quarries are located, bounds the eastern side of the embankment (Fig. 1) and flows into the larger Guadiana river.

A plan view of the tailings deposit is given in Fig. 2. A perimeter dam of increasing height was built over the years as the volume of tailings increased. The figure also shows a representative cross-section of the dam facing the Agrio river, prior to the failure.

The confining embankment was conceived in the original design as a 'downstream' construction rockfill dam, shown in Fig. 3. The embankment was built on top of a thin (4 m) upper granular alluvium covering the marine clays. An upstream blanket of Quaternary clay, covering the slope of the rockfill and connected to a shallow diaphragm wall, was designed to ensure the imperviousness of the embankment.

Manuscript received 8 March 2005; revised manuscript accepted 29 November 2005.

Discussion on this paper closes on 2 October 2006, for further details see p. ii.

* Department of Geotechnical Engineering and Geosciences, Universitat Politècnica de Catalunya, Barcelona, Spain.

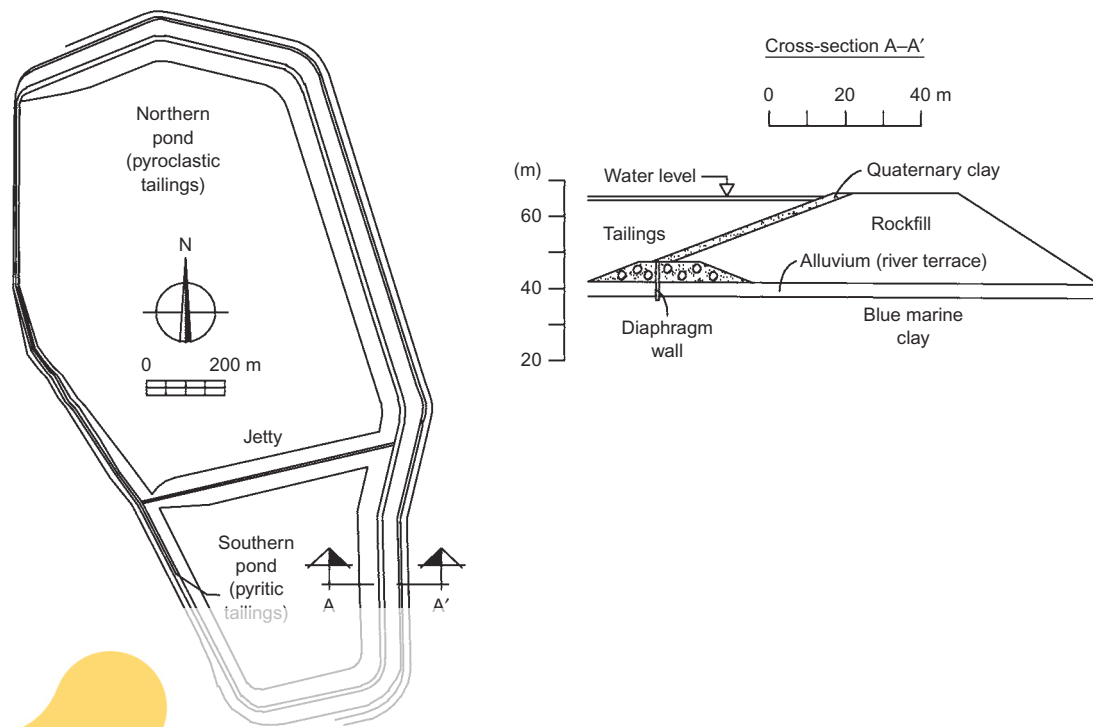


Fig. 2. Plan view of Aznalcóllar tailings deposit and representative cross-section of failed dam

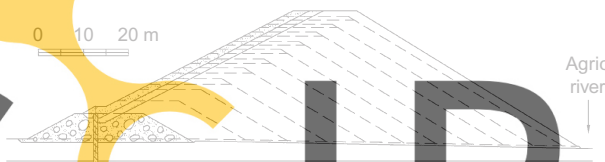


Fig. 3. Original embankment design

As shown in Fig. 2, the lagoon was divided into a larger northern part and a smaller southern one. An inner embankment or 'jetty' was built to separate the two lagoons. Coarse pyroclastic tailings were deposited mainly in the northern lagoon, and finer pyritic slimes were deposited in the southern lagoon. Tailings have been deposited in the lagoons since the beginning of 1978. The height and downstream extension of the embankment increased continuously for 20 years, as the accumulated volume of mine tailings increased. A safety evaluation was carried out in 1996 associated with a modified design that involved raising the height of the lagoon about 2 m above the original design.

Some time during the early morning of 25 April 1998 (when the eastern side of the embankment had a height of 27 m above the foundation) a failure took place involving a substantial section of the confining embankment. As a result, several million cubic metres of highly acid liquefied tailings poured into the Agrio and Guadamar valleys. A 24 km length of the Guadamar river was affected by the mudflow. Fig. 4 shows aerial photographs of the breached embankment, the inundated valley of the Agrio river and the partially emptied and eroded tailings. When these two photographs were taken, in the morning of 25 April 1998, mud and water were still flowing into the Agrio river.

Because of the proximity of the Doñana National Park, which fortunately was protected from the direct flood, this failure had considerable impact on the general public. There was great interest in the case, and several possible causes of the failure were openly proposed in newspapers by people of widely different background and interests. Among the reasons for the failure, phenomena such as the effect of the expansiveness of the foundation clay, chemical attack of the foundation



(a)



(b)

Fig. 4. Two aerial views of the breached dam a few hours after the failure: (a) view from the east; (b) detail of the breach

marls by the acidic pyrite slurry, and the blasting in the nearby open pit mine were all suggested as reasons for the accident.

In fact, it transpired that the causes of the failure were purely geotechnical. Various views have been expressed

concerning the reasons for the failure by geotechnical experts directly involved in the failure, and the discussion continues. As has been the case with other earth dam failures (e.g. Teton dam, Carsington dam), the publication of geotechnical analyses of the failure (Olalla & Cuéllar, 2001) and the associated discussion should aid identification of the reasons for the failure. This is the purpose of this paper, the first of three prepared by the authors, who were expert witnesses in the judicial case that was initiated immediately after the failure. Once a final judgment had been delivered, the authors received authorisation to publish their analyses and conclusions.

In the present paper the failure is reviewed in the context of the geological and geotechnical information obtained from the site and in a laboratory testing campaign, performed at the Department of Geotechnical Engineering of the Technical University of Catalonia. In addition, some background data used in the embankment design and some field observations, prior to the failure, are also reported. In the second paper, the history of dam construction is described and a detailed examination of the failure mechanism is presented, including several different geotechnical analyses. The case is also discussed from the standpoint of current knowledge of failure phenomena in overconsolidated high-plasticity clays. The third paper addresses the events immediately after failure in an effort to integrate post-failure observations into the general understanding of the failure. It also provides an explanation for the distance travelled by the dam after failure and for other related issues such as the speed of the motion and its duration.

GEOLOGICAL OBSERVATIONS

A geological cross-section of the tailings lagoon in a west-east direction is given in Fig. 5. Table 1 summarises the geology of the site. The substrata are Palaeozoic shales

covered by Tertiary deposits: a basal relatively thin pervious unit (gravels, sands and sandstones) and a massive deposit of marine clays, which reaches a thickness of 70 m. Quaternary terraces comprising gravels and sands have been deposited above the Tertiary clays. The embankment reaches its maximum height along the eastern side of the tailings lagoon. The western part has smaller heights because a natural elevation of the ground provided a natural barrier for the lagoon.

The geological description of the site is based on surface observations and on the interpretation of data provided by rotary-drilled boreholes and shallow trenches excavated after the failure in the locations shown in Fig. 6. The displaced area of the embankment, which affected the south-east part of the lagoon, is also shown in Fig. 6. Details of the slide, which was the ultimate cause of the dam failure, are given later.

Boreholes and trenches are associated in groups in order to define better cross-sections or 'profiles' of the embankment at some particular locations. For instance, Profile 1 is defined by boreholes S1-1, S1-2, S1-3 and Trench 4. Profiles 1 and 5 are located outside the displaced area, whereas Profiles 2, 3 and 4 are located within the slide area.

One of the boreholes (S4-3) reached the Tertiary lower sands and sandstones. A piezometer located at this depth found that the water head of the lower sands was at the ground surface, so that the thick deposit of blue clays is bounded by two pervious layers having approximately the same piezometric head.

The Miocene clay cores showed a homogeneous, massive unit. Although structural details are difficult to recognise, two main types of discontinuity were found in the Miocene clay: subhorizontal bedding planes and a vertical jointing system. The difficulty of observing individual bedding planes in this type of clay has been reported previously (e.g. Skempton *et al.*, 1969). However, when freshly cut surfaces

SCIPEDIA

Register for free at <https://www.scipedia.com> to download the version without the watermark

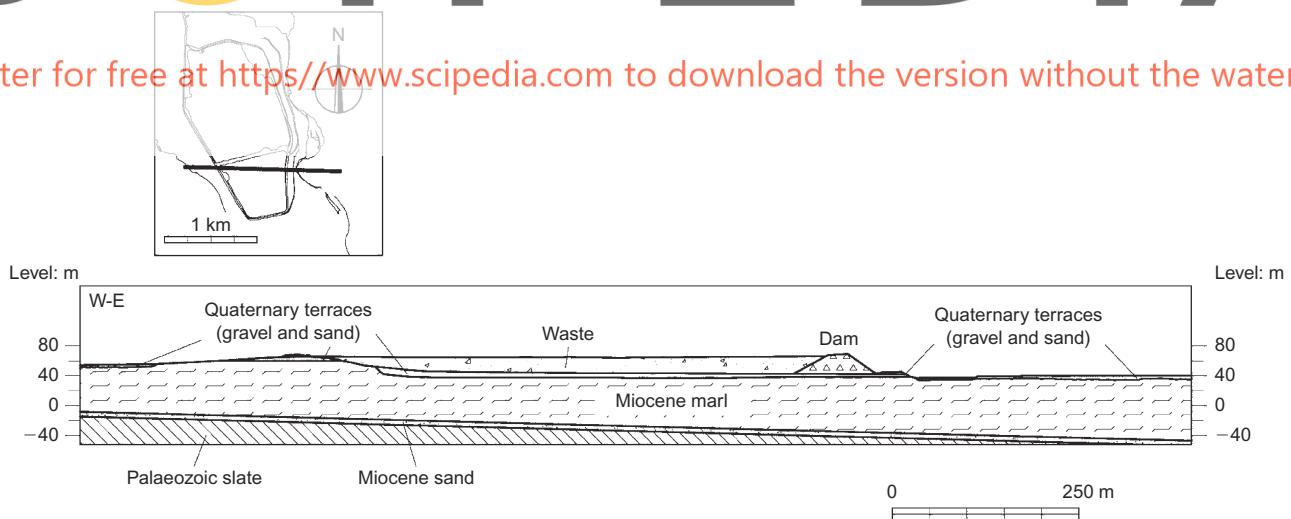


Fig. 5. Cross-section of tailings lagoon. Two stratigraphic discordances are observed: a lower one (high angle) between the Palaeozoic substratum and the upper Miocene deposits, and an upper one (low angle) between the Miocene clays and the Quaternary deposits

Table 1. Soil profile at the location of the Aznalcóllar failed dam

Description	Geological age	Depth: m
Alluvial gravels and sands. Terraces of Agrio river	Quaternary	0–4
Carbonate marine high-plasticity clay (Guadalquivir blue marl)	Miocene	4–75
Gravels, sands and sandstones	Miocene	75–82
Shales	Palaeozoic	>82

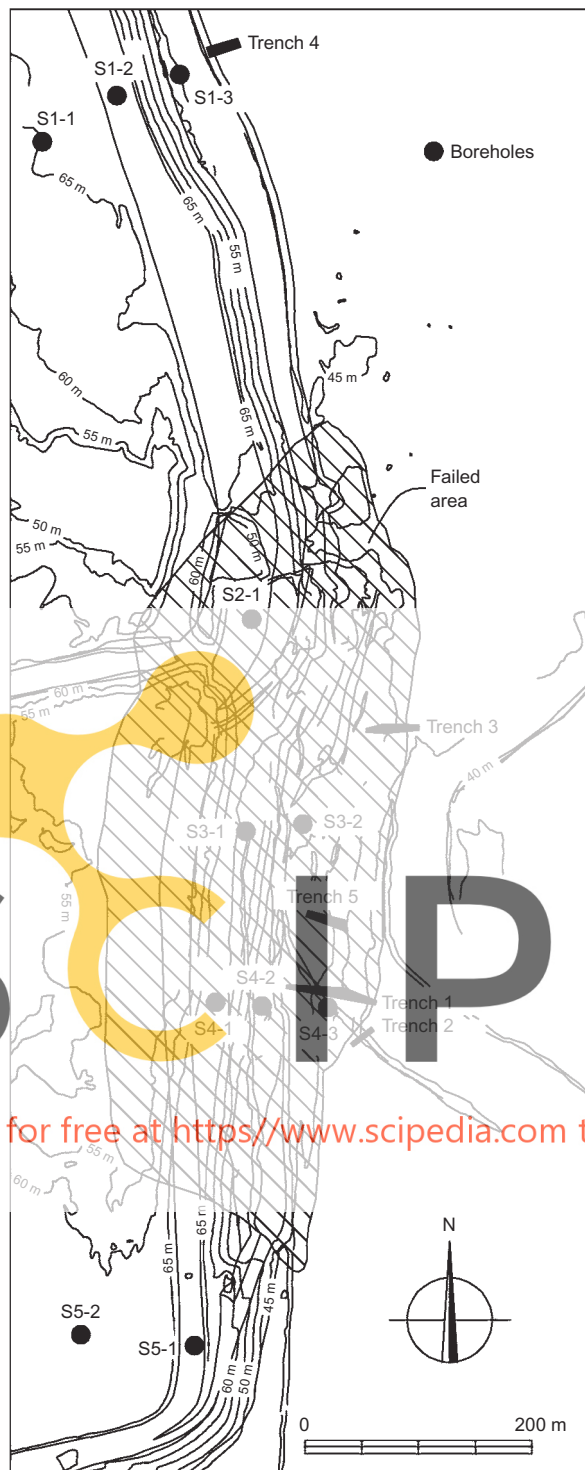


Fig. 6. Location of field investigation boreholes and trenches performed after failure. Displaced area also shown (cross-hatched).

are exposed to the atmosphere and partially dried, some laminations and the alignments of pyrite micronodules reveal the bedding planes (Fig. 7). In exposed outcrops outside the slide area (Fig. 8) the weathered clay exhibits the bedding planes more clearly. A dip of $2-4^\circ$ towards the SSE was measured in outcrops and trenches. Observations in bedding planes, both in outcrops and in cores, revealed some shear striations and some shear zones similar to those described in Chandler *et al.* (1998). Two examples of shear striations are shown in Figs 9 and 10. However, these phenomena were not general, and in other cases the bedding planes appeared

closely sealed and intact. Bedding planes were observed to be concentrated in relatively thin bands at 2.0–2.5 m intervals.

The vertical jointing was easy to observe in outcrops (Fig. 11) and occasionally in cores. The dip is always close to vertical, and the dominant families of planes are oriented N–S and NE–SW. The continuity of these planes is difficult to establish, but is thought to be of the order of 2–5 m with spacing no less than 300–400 mm. These joints are very smooth and often slickensided, with grooves sometimes up to 10 mm in depth. They suggest previous vertical displacements. A review of tectonic studies of the western part of the Guadalquivir basin (Rodríguez Vidal, 1989; Rodríguez Vidal & Flores Hurtado, 1991) indicates tectonic activity dating to upper Miocene, Pliocene and Quaternary periods. These authors suggest that the jointing of the Guadalquivir clays is a consequence of deep active fracturing of the Palaeozoic basement. Tensile phases in the Mio-Pliocene were followed by a compressive stage during the Quaternary period. It is interesting to note that similar vertical joint systems have been identified in other stiff overconsolidated clays, such as London clay (Skempton & Petley, 1967; Skempton *et al.*, 1969) and Oxford clay (Burland *et al.*, 1977; Petley, 1984), although their geological cause may not be the same.

The violent mudflow that followed the breach of the embankment dragged out large blocks of the clay, which floated on the denser tailings mud. One of these blocks is shown in Fig. 12, a month after the failure. It has a remarkable shape, with sharp edges, consistent with the previous description of the clay structure. An oxidation patina is observed on some of the block faces. Despite the strong surface drying suffered by the block, the original water content (as measured in undisturbed core samples) was well preserved once a few outer centimetres of clay were removed. Block samples were recovered from some of these large blocks, which sometimes included distinct joints, for laboratory testing.

The clay was found to be oxidised in its upper 2–5 m. The blue-gray colour of the undisturbed formation becomes brownish near the top of the layer, immediately below the upper sandy alluvium. Traces of oxidation are also found at greater depths in the clay, along the vertically oriented joints.

FIELD OBSERVATIONS PRIOR TO THE DAM FAILURE

Following the recommendations of an evaluation, in 1996, of the dam safety, a monitoring programme was set up. Fig. 13 shows, in plan view, the position of the instruments in the length of the embankment later affected by the failure. Settlement plates, piezometers (in fact observation wells) and a few inclinometers were located along the crest of the embankment (a few fixed points, shown as PF in Fig. 13, were used as a reference for plate levelling). Great significance was assigned to piezometer readings, and a safety procedure was established in the event of piezometers indicating a rise in water pressure or in the case of abnormal outflow. The ‘piezometers’ were slotted open tubes penetrating 2 m into the foundation clay. It is clear that they were not intended to measure pore water pressures in the clay, but rather any water pressures developing in the granular alluvium or in the pervious rockfill.

A visual inspection of the dam was also routinely carried out. A few hours before the failure (in the afternoon of 24 April 1998), an inspection was conducted and the observed state of the dam recorded on an appropriate form, summarised in Table 2. Nothing untoward was detected, but some damage was observed in the instrumentation protec-

Register for free at <https://www.scipedia.com> to download the version without the watermark



Fig. 7. Stratification of clay as observed in a partially dried core (borehole S1-3; depth 19 m)

SCIPEDIA

Register for free at <https://www.scipedia.com> to download the version without the watermark



Fig. 8. Exposed outcrops of Guadalquivir clay showing horizontal bedding planes: river banks of Agrio river



Fig. 9. Slickensides exposed on a bedding plane: river bank of Agrio river

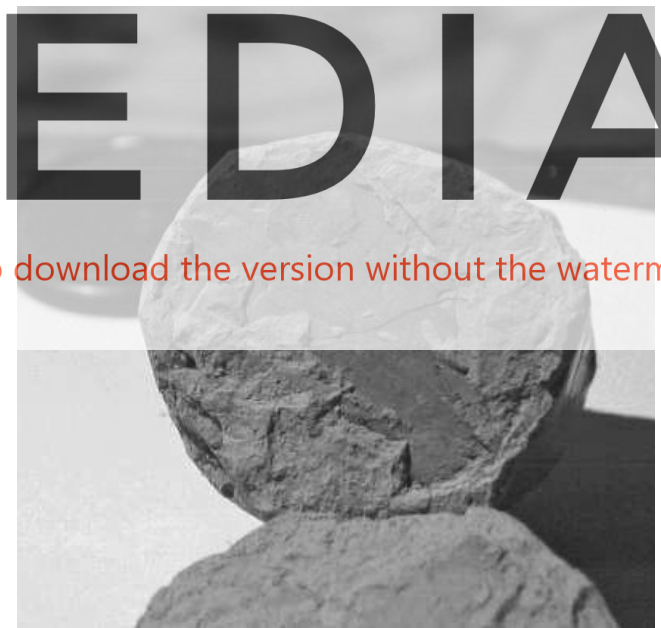


Fig. 10. Slickensides observed in core recovered in borehole S1-3 at 13.5 m depth

tion, which was always in danger of being hit by the large dump trucks used for dam construction.

Inclinometer I-3 was located approximately at the centre of the section of the embankment that slid towards the river at the time of failure. A few readings were made during December 1996–December 1997. They are shown in Fig. 14. The locations of the rockfill/alluvial and alluvial/clay interfaces are shown in the figure. Unfortunately, the upper part of the inclinometer was damaged in January 1998, and no data for the months immediately preceding the failure are available. The displacements shown in Fig. 14 were not



Fig. 11. Vertical jointing: outcrops in Agrio river



Fig. 12. Clay block 'floating' on tailings flow: photograph taken one month after failure

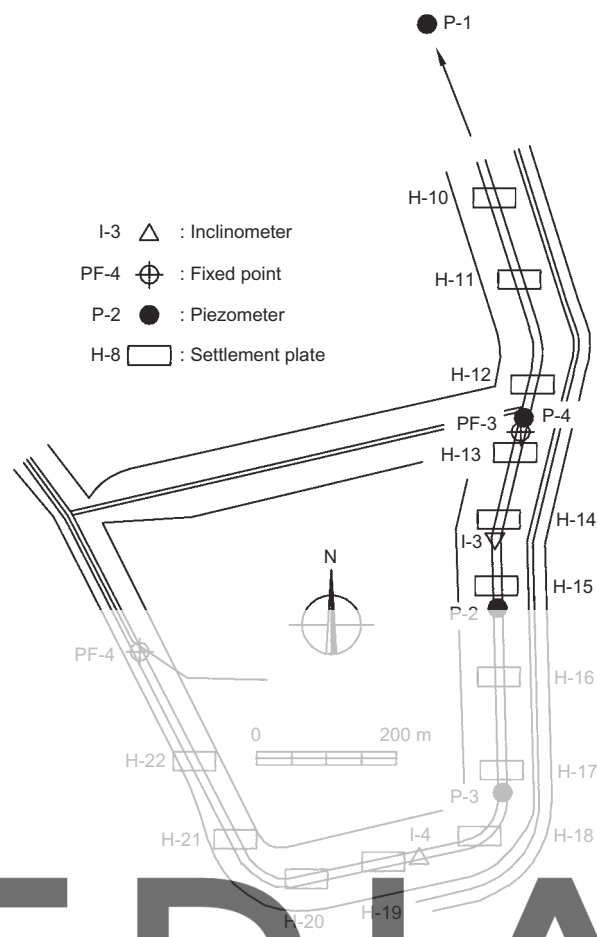


Fig. 13. Position of monitoring instruments: south-eastern side of Aznalcóllar dam

interpreted at the time of readings, as a sign of a possible deep sliding. It was later established, after the failure, that a sliding surface developed at elevation 26 m. Six millimetres of displacements accumulated at this elevation during the year 1997. Most of the observed displacements were recorded within the rockfill embankment, which was under construction.

The recorded water heights of the open tube piezometers P-1, P-2, P-3 and P-4 are shown in Fig. 15. The behaviour is fairly regular during the first 10 months of 1997 and the

recorded water elevation (level 39 m) corresponds to the mid-point of the alluvial layer. After November 1997 the measurements show a more irregular pattern difficult to interpret. The last available readings, in April 1998, indicate that the water level was again within the limits of the pervious granular alluvium. No abnormal settlements were recorded. Horizontal displacements of the embankment, however, were not measured. The behaviour of the dam was always considered normal, and the regular monitoring reports did not express any special concern.

Table 2. Aznalcóllar tailings lagoon: visual inspection form

Date	24-4-1998
Weather conditions	Sunny
Weather conditions during the past 15 days	Cloudy, rainy
Inspection of embankment crest. Observations made	Nothing relevant is observed. Occasional trucks carrying red clay*
Inspection of embankment foot. Observations made	Everything is quiet. No anomalies observed. Trench totally dry.† There is a pump intermittently running in the south-eastern corner
Did you notice cracks or surface instabilities in the ground?	No
Is there any damage to the monitoring instruments?	Yes
Water level in the lagoon	$B = 7$; $A = 4.4^\ddagger$
Other data. Comments	Fixed point PF4 is inclined (inclined concrete tube) Tubes for monitoring instruments protection have been added Modified settlement plates not yet installed

*Red clay was used to build the upstream impervious blanket.

†A trench running parallel to the embankment foot collected water and was used to monitor flow, eventually escaping the lagoon.

‡This refers to the distance from the dam crest to the lagoon free water table at two positions in the western part of the embankment.

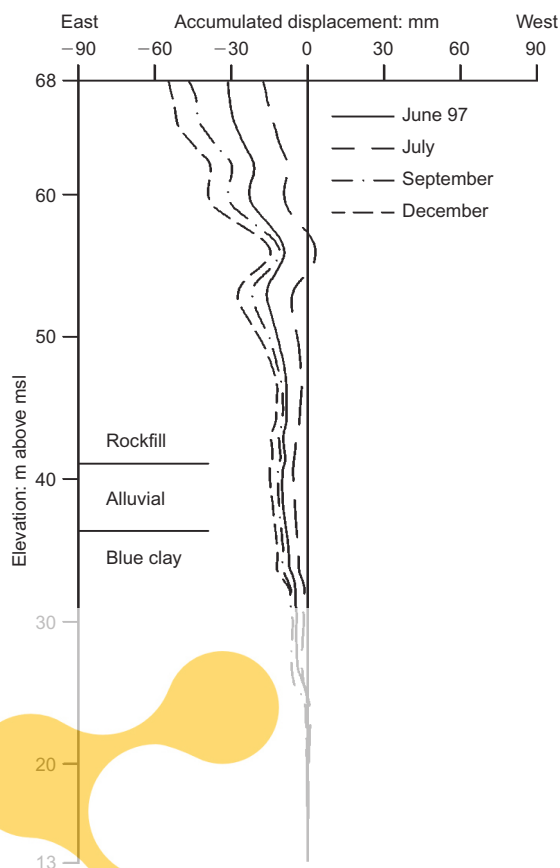


Fig. 14. Readings in inclinometer I-3 in direction perpendicular to dam axis (towards the east)

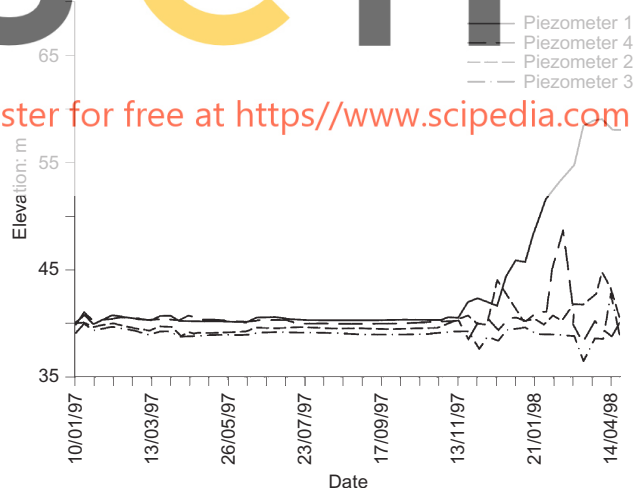


Fig. 15. Evolution of water elevation in piezometers P-1, P-2, P-3 and P-4

GEOMETRY OF THE FAILURE

It became clear soon after the failure that a translational movement was the reason for the breach that opened in the embankment. There was no evidence of other possible mechanisms, such as overtopping of the embankment, instability of the embankment slopes or internal erosion. A comparison of topographic maps before and after the failure (Fig. 16) was crucial in this regard.

The investigation first considered the geometry of the slide; then the strength properties of the dam, the tailings and, especially, the foundation were established. Finally, a

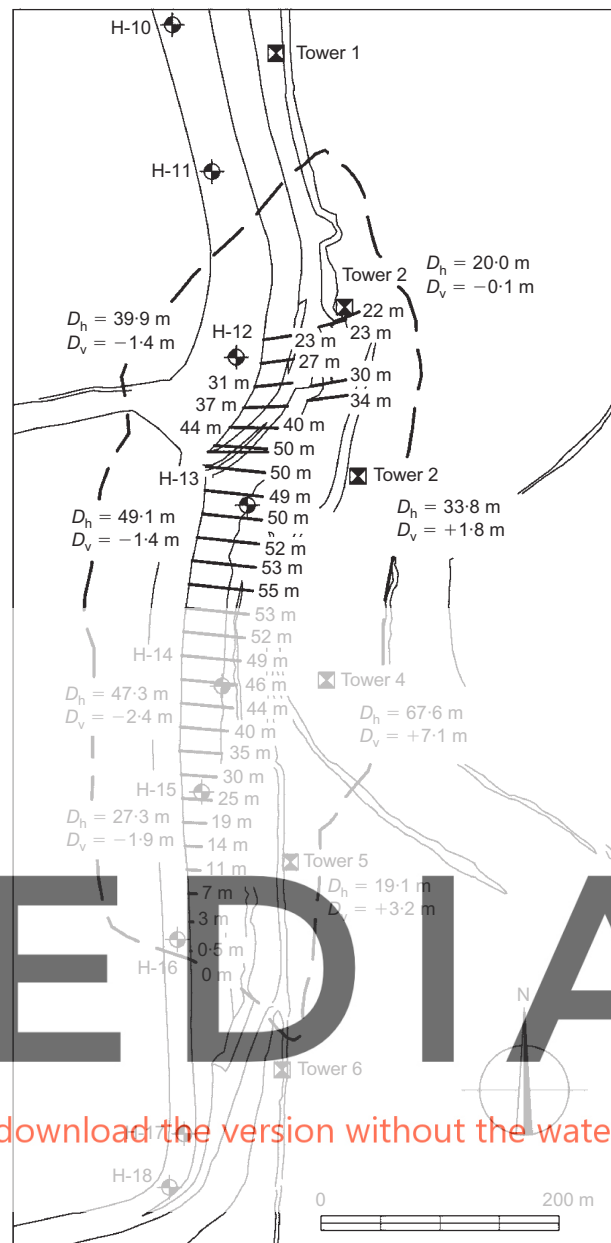


Fig. 16. Limits of the slide area and vectors indicating the displacement. Displacements were measured in topographic marks and electrical towers. D_h , horizontal displacement; D_v , vertical displacement (negative numbers indicate a drop in elevation)

consistent geotechnical model able to integrate the measured properties and field observations has been devised.

The breach in the embankment immediately north of the jetty that divided the northern and southern lagoons was a direct consequence of a deep translational slide, south of the breach, which displaced 600 m of embankment and its foundation towards the east. The failure surface was located inside the blue clays. The displaced mass included the embankment, the alluvium terrace and about 10 m of the blue clay. Fig. 17 shows the cross-section of the slide at the position of Profile 4, defined by boreholes S4-1, S4-2 and S4-3 (see location in Fig. 6). The section in Fig. 17(a) includes data provided by all the boreholes shown in the figure. Some of the boreholes shown were performed by other parties involved in the post-failure investigations. The boreholes located upstream of the embankment provided a precise position of the failure surface, as the tailings were

Register for free at <https://www.scipedia.com> to download the version without the watermark

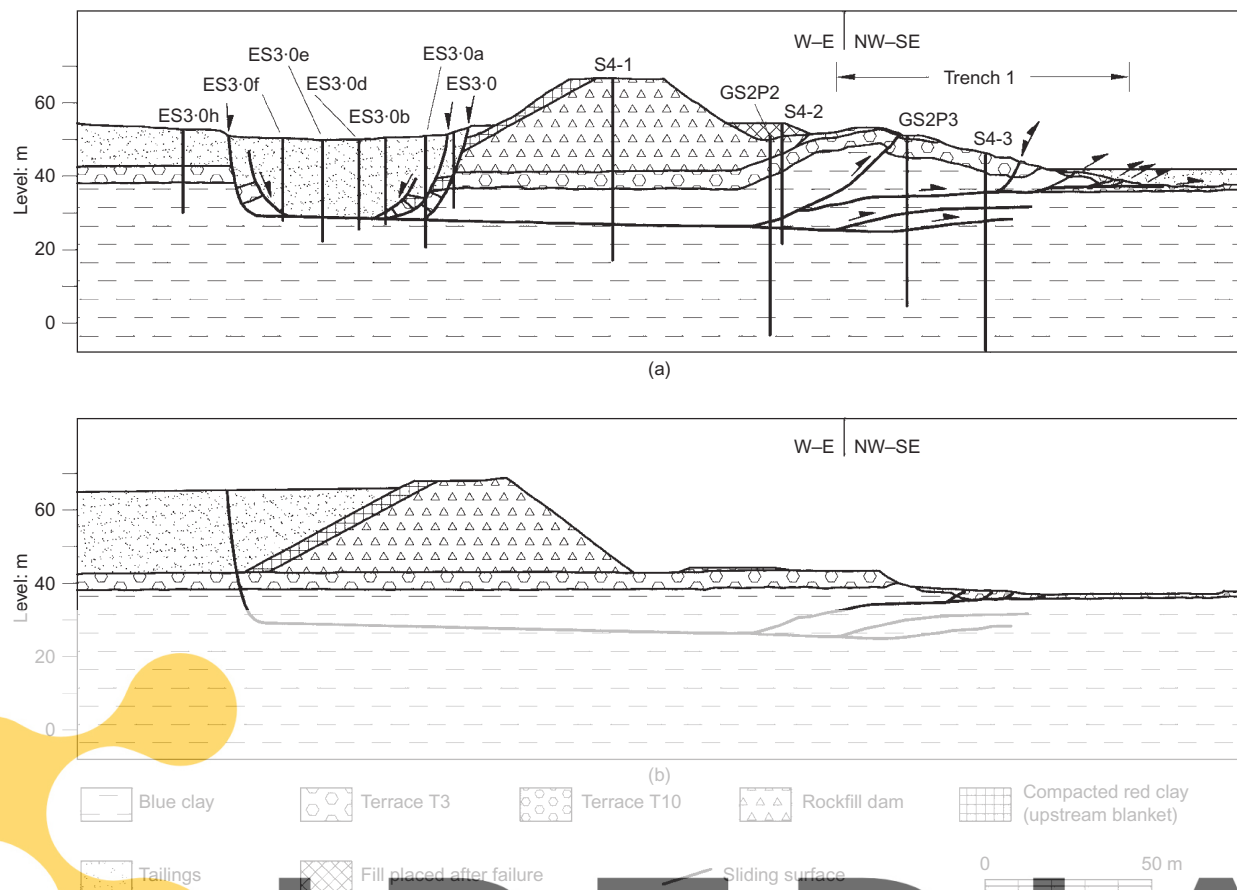


Fig. 17. Cross-section of slide at position of Profile 4: (a) geometry after the slide, as interpreted from borehole results and surface topography; (b) reconstruction of position of sliding surfaces before failure

found in direct contact with the clay in some of them (e.g. Boring ES3-0e in Fig. 17). In several boreholes it was also possible to identify the position of the sliding surface where a highly polished surface could be found. This is the case for the plane shown in Fig. 18.

Also indicated in Fig. 17(a) are the folded structures found at the foot of the downstream slope of the embankment. The interpretation given is based on zones of intense shearing found in boreholes and trenches. Upward displacements of the ground, close to 8 m, were measured at the position of the folded strata. Fig. 17(b) provides a reconstruction of the original position of the sliding surface before failure displacements. An interesting finding of this reconstruction is that the head scar of the slide was a near-vertical surface located at the original upstream toe of the embankment. This vertical scar was fairly well preserved even after the intense erosion of the tailings deposits that followed the uncontrolled flow out of the lagoon. This is shown in Fig. 19.

It was also observed that the tailings could maintain stable vertical cliffs 15–20 m high (Fig. 20). The position of the initial upstream vertical scar, as given by the reconstruction of the original profiles, is shown in Fig. 21. Also shown in this figure is the position of the scar, some months after the failure. It shows a small retrogression towards the lagoon as a consequence of (limited) sliding and erosion. The vertical jointing on the clay foundation is consistent with this interpretation of field observations as it explains the existence of a nearly vertical upstream limit of the slide, within the blue clay, which continued upwards within the tailings deposit.

Observations made a few hours after the failure showed small mud volcanoes on the solidified tailings upstream of

the dam (Fig. 22). This was a clear indication of tailings liquefaction during the failure process.

The inclination ($1.5\text{--}2^\circ$) and planar nature of the basal sliding surface are a strong indication that it followed a bedding plane. The position of settlement plates, precisely located on the crest of the embankment before the slide, could be used also to determine the horizontal (D_h) and vertical (D_v) displacements experienced by those plates. The measured values are indicated in Fig. 16. The slope ($\arctan D_v/D_h$) is also consistent with a sliding surface dipping $2\text{--}3^\circ$ towards the east. A comparison of the topography before and after the failure also provides a good indication of the magnitude of horizontal displacements (Fig. 16).

The central part of the embankment moved 40–55 m towards the east (directions varied between 93° and 100° with respect to north). The magnitude of the displacement decreased to 20–22 m at the northern limit of the slide, at the position of the open breach. Towards the south, a more gradual decrease of displacements was observed. In total, a 600 m long portion of the south-eastern embankment of the lagoon was affected by the slide. North of the breach, no displacements of the embankment were detected.

The shape of the northern limit of the slide (Fig. 16) suggests that the failure surface crossing the embankment was controlled by the dominant orientation (NE–SW) of the vertical joints of the foundation clay. An interpretation of the original rupture breach is given in Fig. 23. The orientation of the embankment, its size, the direction and intensity of the sliding motion and the orientation of the rupture plane led to an initial breach width of 14 m. Note also that the two lips of the breach separated immediately, and therefore



Fig. 18. Highly polished and striated shear plane that follows a bedding plane (S_0). Borehole 2-1 at 33.8 m depth. It was interpreted as belonging to the sliding surface

no shearing resistance was offered by the rockfill embankment. Given the width of the embankment at the position of the breach (crest width 45 m), a shear distortion amounting to 10 m of displacement could probably have been resisted by the embankment, avoiding the opening of a free outflow for the tailings.

The orientation of the initial outflow is indicated by the depositional fans observed outside the breached embankment (Fig. 4(b)). The flow of tailings was directed initially in a NE direction, against the natural slope of the Agrio valley. Later, the progressive erosion of the breach allowed the outflow to change direction towards the east.

GEOTECHNICAL PROPERTIES OF MINE TAILINGS

During the mining process, the rock minerals are first crushed and then finely ground in a wet process in order to



Fig. 19. The straight line, indicated by arrows, shows the position of the upstream scar of the slide



Fig. 20. Vertical cliffs inside lagoon as observed a few weeks after failure

separate the metallic minerals. The finely milled waste, after processing, is pumped in aqueous suspension to the disposal lagoon. The tailings mud contains pyrite, other metallic minerals and some additional compounds (oxides, calcium sulphate and chemical reactives). The free water in the lagoon is acid (pH 3–3.7) and has a high concentration of dissolved solids. The southern lagoon received finer pyritic material (silt size). The larger northern lagoon received more heterogeneous, often coarser (fine sand size) material, particularly during the early stages of waste deposition, which is described as 'pyroclastic'. Undisturbed samples were recovered in two boreholes (S1-1 in the northern lagoon and S5-2 in the southern lagoon) and in a few block samples taken from the exposed tailings cliffs inside the lagoon. These operations were performed in September–October 1998, a few months after the failure, after the water level in the lagoon had been reduced to a low level. Samples taken in the southern lagoon remained saturated, though the coarser materials sampled in borehole S1-2 were often unsaturated. Fig. 24 shows the distribution of average grain size with depth determined in the two lagoons.

The pyritic lagoon, which was directly involved in the sliding, contains remarkably homogeneous material with a grain size distribution ($C_u = 4.7$) as shown in Fig. 24(b). The heavy pyritic mineral ($\gamma_s = 4.3 \text{ g/cm}^3$) results in a high saturated specific weight ($\gamma_{\text{sat}} / \gamma_w = 3.1$). The variation of void ratio with depth, for all the specimens tested, is shown in Fig. 25. Large variations in density are found, though the southern lagoon appears to be more homogeneous ($e = 0.5\text{--}0.8$). A scanning electron micro-

Register for free at <https://www.scipedia.com> to download the version without the watermark

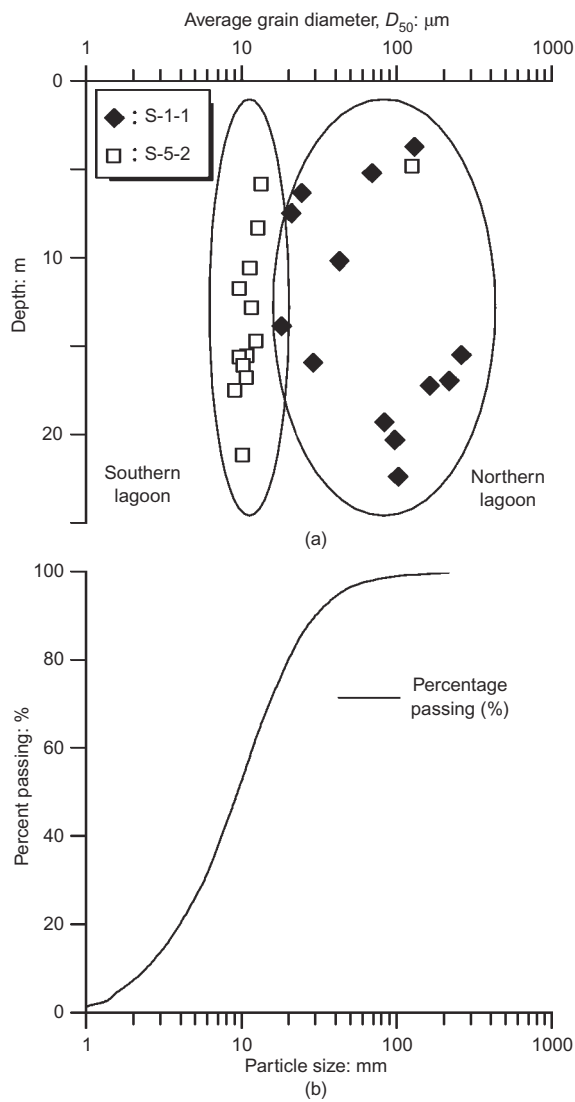


Fig. 24. (a) Average grain sizes of deposited waste; (b) particle size distribution of pyrite tailings (southern lagoon)

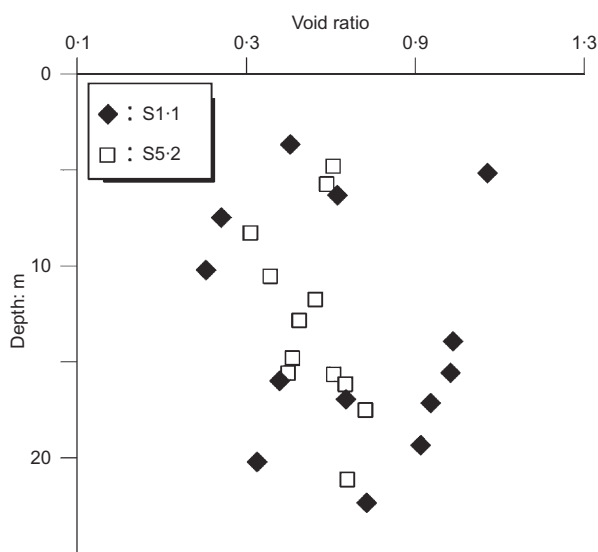
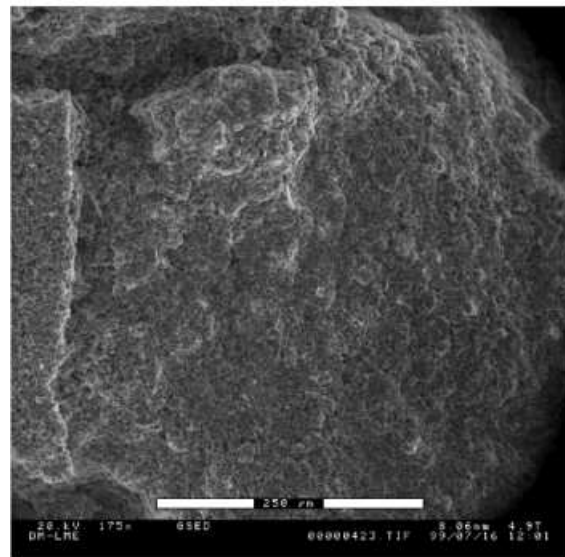


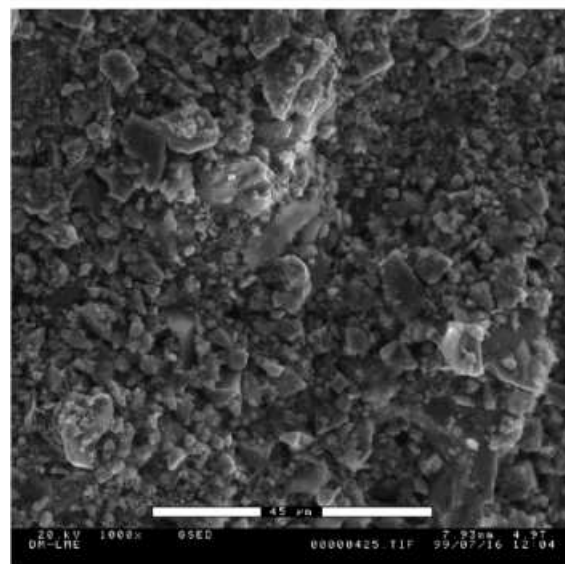
Fig. 25. Variation of void ratio with depth: northern (S1-1) and southern (S5-2) lagoons



(a)



(b)



(c)

Fig. 26. (a) Specimen of pyrite tailings after triaxial testing; (b) view at $\times 175$ scale; (c) view at $\times 3000$ scale

22.00 m in borehole S5-2 (southern pyritic lagoon). The initial void ratio, e_i , was 0.733. Specimens were consolidated to the estimated effective initial stress. The undrained application of the deviatoric stress resulted in an initially stiff

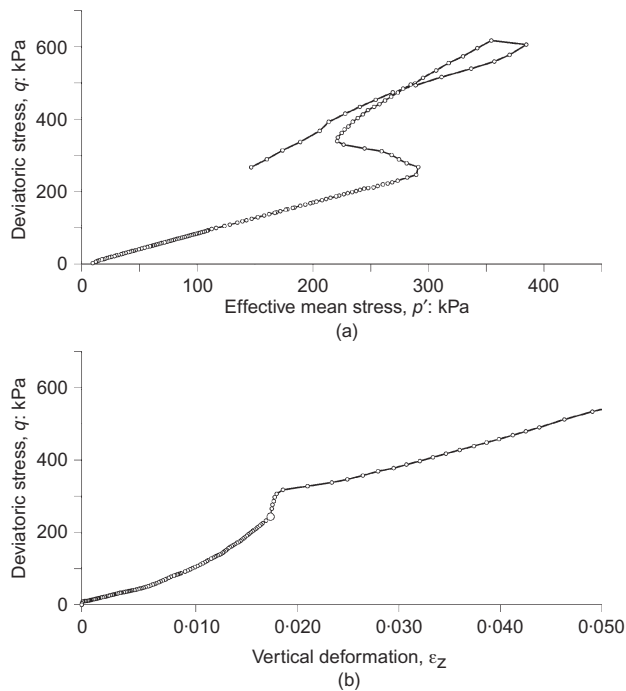


Fig. 27. Undrained K_0 consolidated ($K_0 = 0.5$) triaxial test on specimen M9 from borehole S5-2 (southern lagoon): (a) effective stress path; (b) deviatoric stress–vertical strain response

response and a rapid generation of pore pressure, indicating a collapse of the granular structure. However, as failure conditions were approached, a strong dilatancy changed the trend of pore pressure generation, and the path followed the strength envelope at increasing effective confining stress. When the test was stopped, at very large strains (24%), positive pore pressures were again recorded, although they may not be very significant in view of the large strains reached. Failed specimens, especially those coming from the pyritic lagoon, showed distinct shear planes.

Failure conditions were homogeneous with depth. Fig. 28 shows the strength, q_f , found for specimens taken in borehole S5-2, within the southern lagoon. Also shown is the position of all specimens recovered. Undrained strength of the pyritic waste increases at a rate $q_f/\sigma'_{\text{initial}} = 0.8$, where q_f corresponds to the maximum value of generated pore water pressure. The range of effective friction angles determined in tests on both pyritic and pyroclastic materials is $37\text{--}42^\circ$. No correlation with grain size (D_{50}) or void ratio could be identified.

Evidence of cementation

Direct shear tests on 60 mm diameter specimens were also performed on saturated specimens. Peak conditions are given by the parameters $c' = 17$ kPa, $\phi' = 41^\circ$. At the end of the tests, for a displacement of 6 mm, c' and ϕ' drop to $c' = 0$ and $\phi' = 41^\circ$. The stress–displacement curve of a test performed on specimen S5-2/5, under a vertical stress $\sigma'_v = 200$ kPa, is shown in Fig. 29. A peak and a subsequent moderate reduction of strength are observed.

A few unconfined compression tests on samples taken in the pyritic lagoon were also performed. Care was taken to saturate the specimens before testing. The measured variation of q_u with depth is shown in Fig. 30. No clear trend is observed, but the significant result is that strengths in the range 100–200 kPa are measured in the central part of the deposit. In all samples a failure plane developed, inclined at

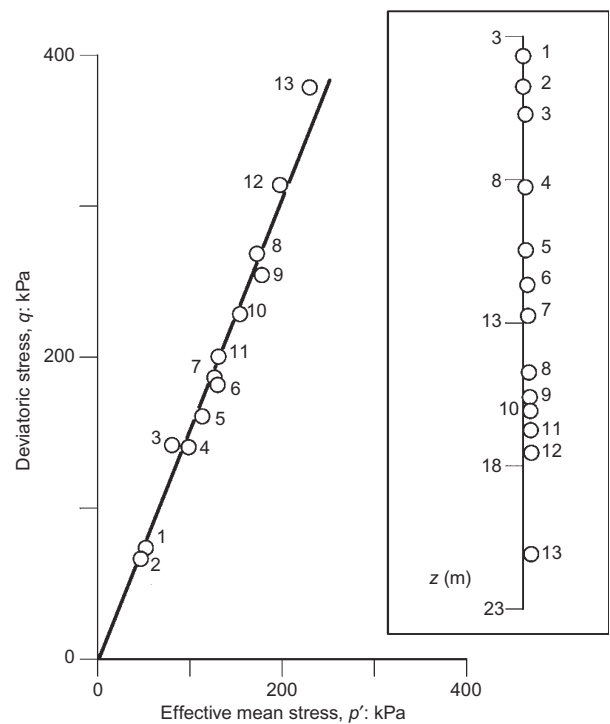


Fig. 28. Variation of undrained shear strength with depth of pyritic waste

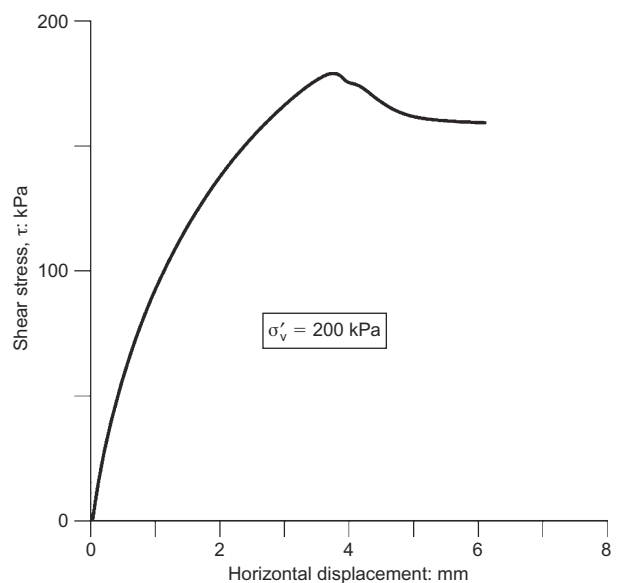


Fig. 29. Direct shear test in sample S5-2/5

$60\text{--}70^\circ$ with respect to the horizontal plane. A marked peak was observed in all cases.

Oedometer tests were also performed on samples from the southern lagoon. Measured vertical permeabilities for the pyritic tailings ranged from 10^{-6} to 10^{-7} m/s, a rather low value consistent with the grain size distribution. Values of c_v increased significantly with vertical stress (Fig. 31), a result that is interpreted as an indication of the progressive deterioration of specimen cementation. A similar trend was observed in the values of the permeability and in the coefficient of secondary compression. Confined stiffness moduli were found to be higher for the deeper (and therefore older) specimens (Fig. 32), a result that is also an indication of cementation effects.

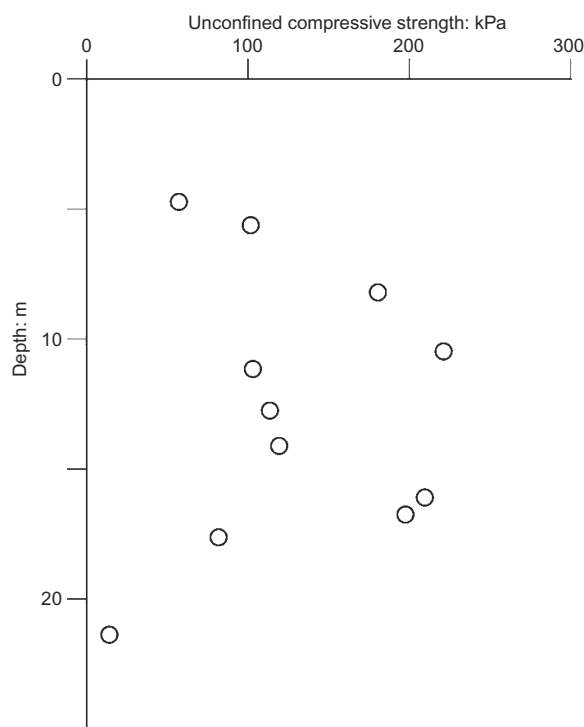


Fig. 30. Unconfined compressive strength of saturated samples from pyritic deposit

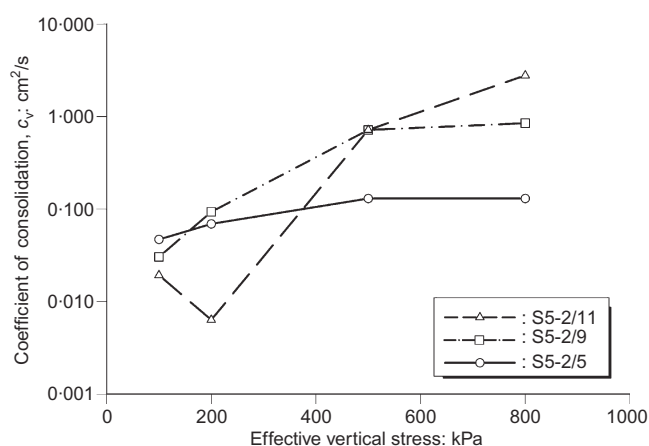


Fig. 31. Oedometer tests on pyritic specimens: variation of coefficient of consolidation with vertical stress

In summary, the pyrite tailings are described, from a geotechnical point of view, as a homogeneous and poorly graded silt of high density owing to the dense pyrite particles. The deposition process leads to a heterogeneous distribution of void ratios ($e = 0.5-0.8$). This granular soil has developed a degree of cementation since it was deposited. Cementation increases with age and therefore with depth, but it is destroyed as shear or confining stresses are applied. Undrained triaxial compression at slow rates of loading is not capable of inducing static liquefaction, a consequence of dilatancy in the proximity of peak strength. Friction is high when measured in triaxial tests ($\phi' = 38^\circ$) and in shear box tests ($\phi' = 41-42^\circ$). The low measured permeability favours an undrained field response of the materials. The coarser pyroclastic materials (classified as poorly graded fine sands) of the northern lagoon are more pervious, but their behaviour in undrained triaxial testing is similar to that of the pyritic mud.

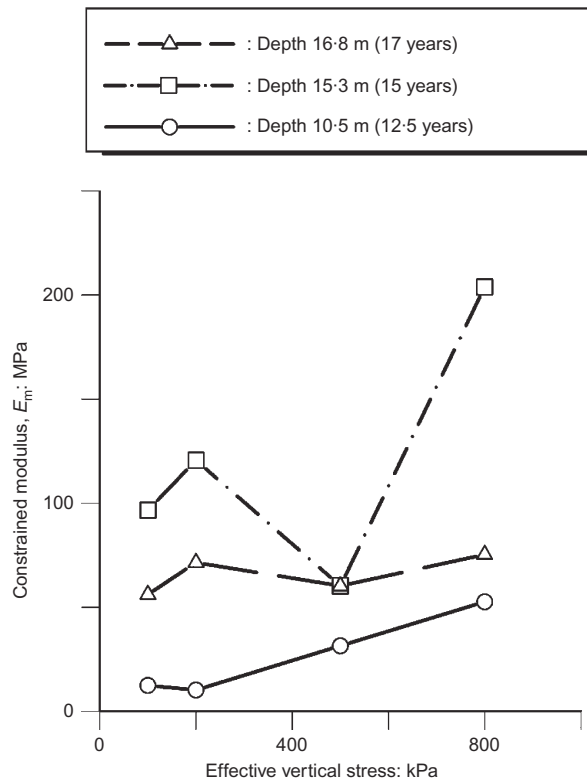


Fig. 32. Oedometer tests on pyritic specimens: variation of confined moduli with age of specimen and vertical stress

GEOTECHNICAL PROPERTIES OF THE FOUNDATION CLAY (BLUE GUADALQUIVIR MARL)

It was decided to test in some detail two 'soil columns': boreholes S3-1 and S4-1 located in the slide area (Fig. 6). These two boreholes encountered first the embankment rock-fill, then the alluvial layer and finally the blue clay. The detailed stratigraphy of a portion of the blue clay, from borehole S3-1, is shown in Fig. 33. The sliding plane was estimated to be located at elevations 26–27 m. In one location a warped bedding plane was identified. Subhorizontal laminations (dip $1-2^\circ$) presumably parallel to bedding planes were also observed. Shear bands were also detected at non-regular intervals. They are often inclined at a significant angle. Pyrite micro nodules are scattered throughout, often showing linear arrangements parallel to bedding or lamination planes.

Some samples taken from borehole S1-2, outside the slide area, were also tested in order to evaluate the homogeneity conditions at a larger scale. Additional tests were performed in block samples taken from the large clay blocks deposited by the mudflow in the debris fan adjacent to the dam breach (Fig. 12).

Basic identification

The samples tested exhibit a high percentage of clay sizes ($< 2 \mu\text{m}$) using standard sedimentation techniques. The clay fraction varies between 47% and 58%: average 53%. They classify as MH or CH ($w_L = 62-67\%$; $I_p = 31-35\%$). The activity is therefore moderate ($A = 0.62$). The particle specific weight was constant ($\gamma_s = 2.71-2.72 \text{ g/cm}^3$). Water content is plotted in Fig. 34 against depth. No significant trends are identified in the upper 20 m of clay. Some of the samples recovered had abnormally high water contents. They correspond to muddy parts found at the upper ends of some of the samples recovered, probably as a consequence of drilling operations. The scatter of water content in undisturbed speci-

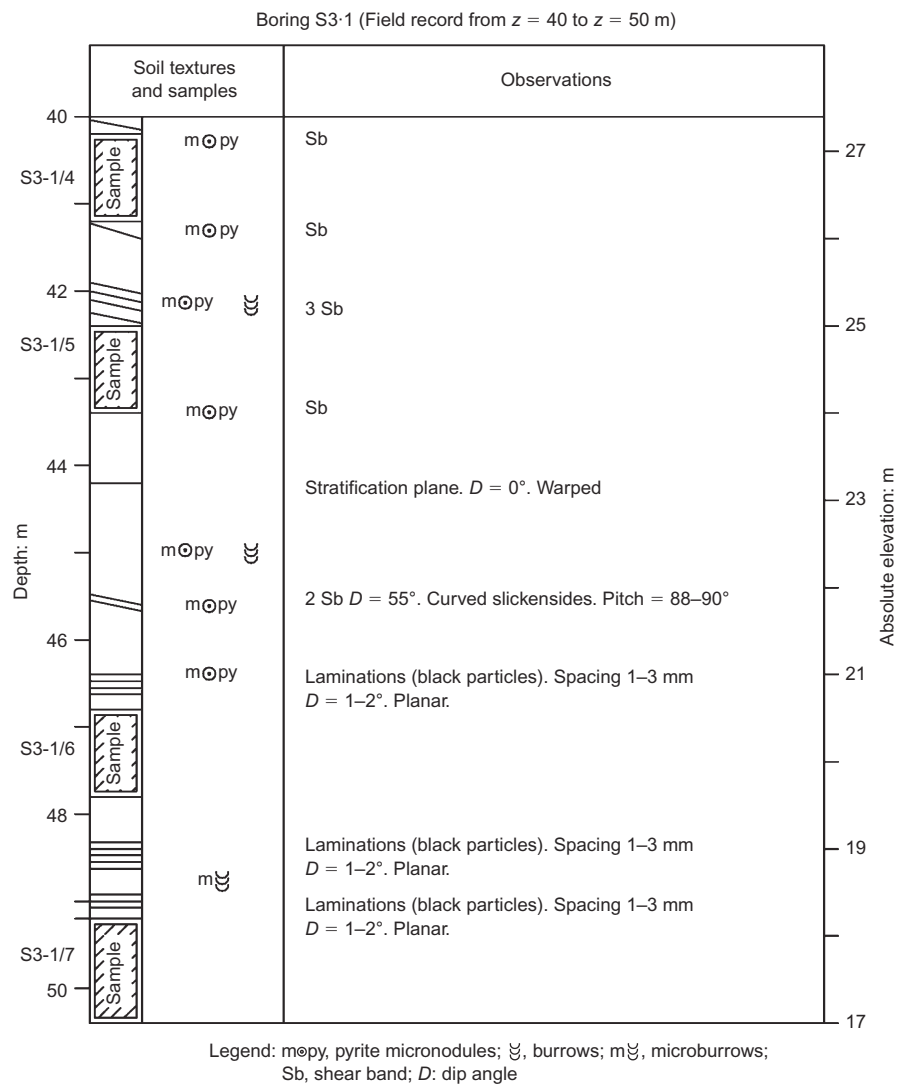


Fig. 33. Portion of stratigraphic column of borehole S3-1 between depths $z = 40$ m and $z = 50$ m (location of borehole shown in Fig. 6)

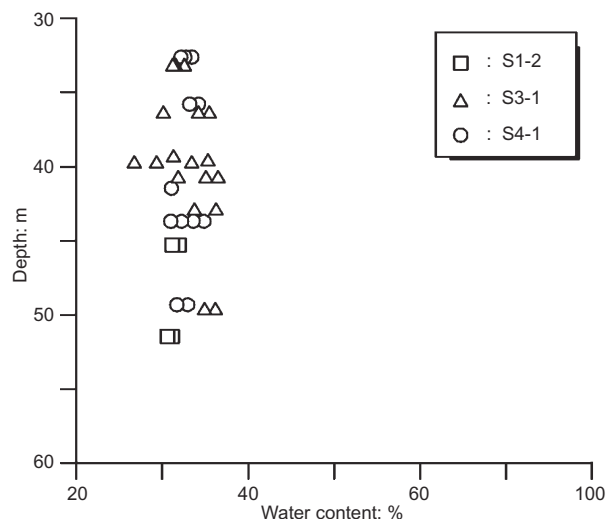


Fig. 34. Measured values of water content in Guadalquivir clay foundation

mens is in the range 30–35%, which corresponds to void ratios in the range 0.81–0.95. Natural densities varied in the range 1.90–1.98 g/cm³. At the scale of the problem, the foundation soil appears essentially uniform.

Mineralogy and structure

In X-ray diffraction tests calcite and quartz were identified as the non-clay minerals, amounting to roughly 30% of the total mineral content. Calcite and potassium smectite constitute the bulk of the clay mineral content; minor proportions of illite and kaolinite are also found. Other studies (Tsige, 1998) of the mineralogy of the Guadalquivir clay found similar results. Previous experience (Alonso *et al.*, 1992) indicated that sliding surfaces may exhibit some changes in mineralogy when compared with the soil matrix. As a consequence, powder samples were taken from the surface of discontinuities found in the large blocks described previously (Fig. 12). There was, however, an almost complete similarity between the mineralogical contents of the matrix and those of the exposed surface specimens. Only the amount of iron changed, which explains the change in colour. It is presumed that this minor change is associated with flow processes along open fissures in the upper levels of the clay unit.

Scanning electron microscope observations were made on intact samples (by examining a surface induced by a tension failure) and on sheared surfaces. In all cases the clay minerals were seen to occur in aggregates of irregular ellipsoidal shape, having sizes of 5–10 μ m (Fig. 35). Weathering (brownish colours) results in a more marked aggregate structure. Tsige (1998) found that the weathered clay had an

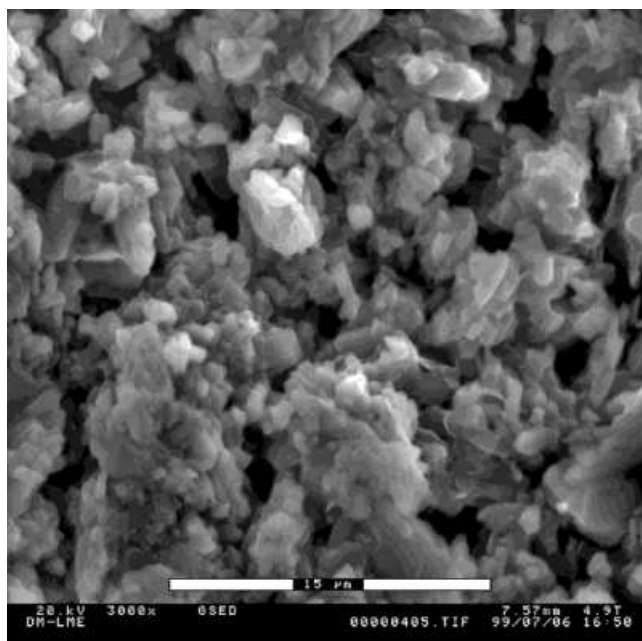


Fig. 35. SEM microphotograph (×3000) of a discontinuity surface of the blue clay

increased percentage of larger pores and a reduced plasticity.

A significant proportion of the calcite content relates to the fossilised microfauna, which is disseminated through the clay mass. This explains the relatively low cementation found in this marly clay.

Direct shear on specimens recovered in boreholes

Specimens 50 mm or 60 mm in diameter and having thicknesses of 26 mm were tested in shear boxes previously calibrated in order to compensate for deformations not induced on the clay. Tests were performed in groups of three specimens, cut from a given sample, and subjected to three different vertical effective stresses, in the range 100–800 kPa. It is shown in a companion paper that the vertical effective stresses in the basal sliding plane varied between 100 and 350 kPa at the time of failure. Shearing was commenced once the consolidation reached the secondary consolidation stage. The shearing speed was less than 0.005 mm/min to ensure approximate drained conditions. The results are summarised as follows.

- (a) All the specimens exhibited a brittle behaviour. Peak strength was found for displacements of 0.5–1.5 mm (for a range of vertical stresses of 100–400 kPa). Beyond peak the strength initially drops rapidly, then more gradually. This behaviour is illustrated in Fig. 36 for one of the specimens tested. This behaviour will be described by the following parameters: peak strength, τ_p ; displacement to reach the peak, d_p ; strength at the end of the test (for a displacement of 4–6 mm), τ_f ; rapid drop of resistance post-peak: $\Delta\tau_b$. An additional reference strength, the residual strength τ_{res} , may be calculated for a given vertical stress once the residual friction angle is known. As shown later, a representative value $\phi'_{res} = 11^\circ$ was found for this clay. Two brittleness indices are used: $I_f = (\tau_p - \tau_f)/\tau_p$ and $I_B = (\tau_p - \tau_{res})/\tau_p$. I_B is the definition proposed by Bishop (1967). It is clear that $I_B > I_f$. In addition, a measure of the rapid loss of strength after the peak is given by the cementation loss indices, $CL_f = \Delta\tau_b/(\tau_p - \tau_f)$ and

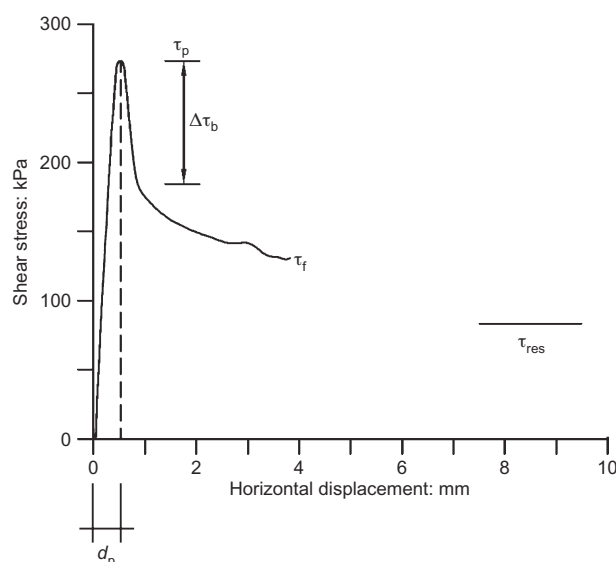


Fig. 36. Direct shear test on specimen of foundation clay from sample M3, borehole S3-1 (depth 39.20–40.1 m): normal effective stress 400 kPa

$CL_B = \Delta\tau_b/(\tau_p - \tau_{res})$, proposed here. They have been associated with the shear-induced loss of cementation of the clay. Again, the first ‘cementation loss index’ is larger than the second ($CL_f > CL_B$).

- (b) The ‘cementation loss’ indices are plotted in Fig. 37, for all the specimens tested, against the vertical stress. No apparent effect of vertical stresses is observed. Average values are very significant ($\bar{CL}_f = 0.55$; $\bar{CL}_B = 0.35$). They indicate that a large proportion of the peak strength is lost immediately. If the residual strength is taken as the final reference minimum strength value, it is suggested that 35% of the loss of strength after peak is due to the loss of cementation, and a further reduction of 65% is associated with changes of the fabric of the clay (particle reorientation).

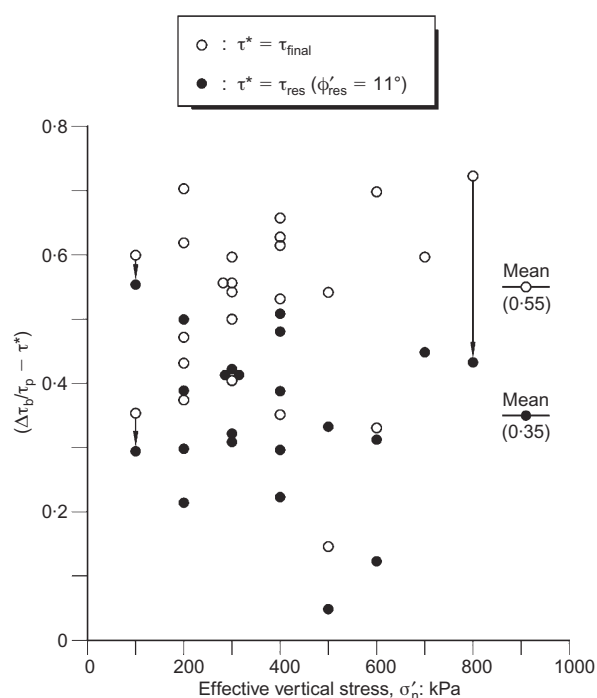


Fig. 37. Normalised loss of strength of foundation clay, immediately post-peak, as a function of vertical stress

- (c) The displacement at peak, d_p , does not change with the applied normal effective stress (Fig. 38). The average value of $d_p = 1$ mm. The two brittleness indices I_f and I_B are also plotted in Fig. 39 against the vertical stress. A single I_B line is plotted in Fig. 39 because the residual strength corresponds in all cases to a common residual friction angle ($\phi'_{res} = 11^\circ$) and peak strength values derive from a common peak strength envelope ($c' = 65$ kPa, $\phi' = 24.1^\circ$; see below). Points in Fig. 39 represent the I_f index determined for each of the shear tests performed, and this leads to the scatter observed. The dashed line provides the mean value of I_f . A reduction of brittleness with vertical stress is observed, a common finding also in other soils (Fig. 40). The important point is that the Guadalquivir blue clay is highly brittle (I_B varies between 0.8 and 0.7 for effective vertical stress between 100 kPa and 400 kPa). Measured brittleness indices are similar to the values found for blue London clay (Bishop *et al.*, 1971; Fig. 40).
- (d) In all direct shear tests performed in samples recovered in boreholes there was no clear evidence that a distinct bedding plane was sheared. Therefore the measured

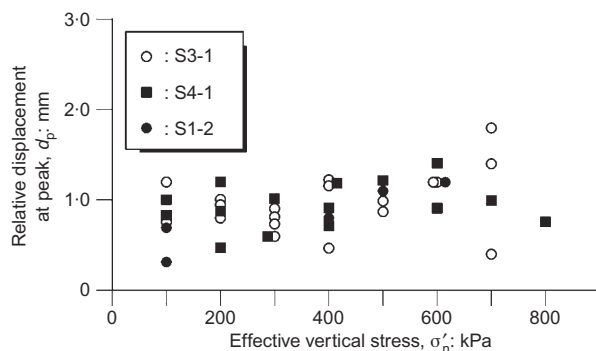


Fig. 38. Variation of peak displacement with effective normal stress for foundation clay

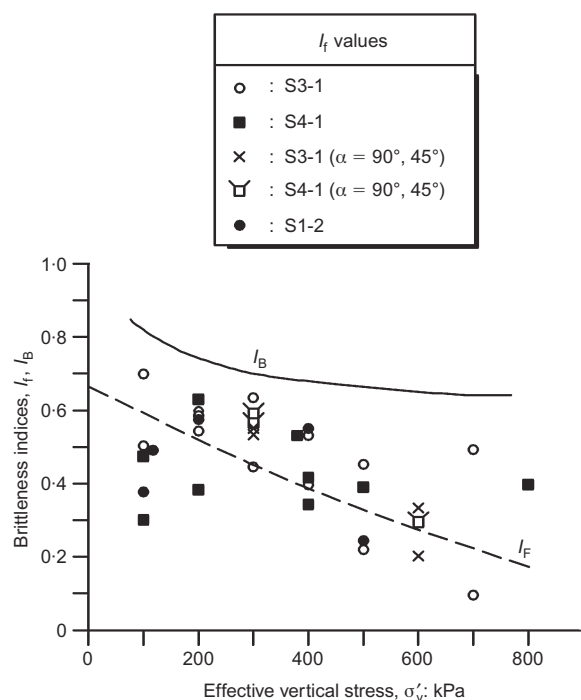


Fig. 39. Variation of brittleness indices I_B and I_f of Guadalquivir blue clay with effective vertical stress

strength on horizontal planes corresponds to the clay matrix. Measured peak strengths are plotted in Fig. 41 in a Coulomb diagram. Some scatter is observed. Average peak strength values correspond to the drained parameters $c' = 65$ kPa, $\phi' = 24.1^\circ$. If the strengths measured at the end of the direct shear test (for displacements of 4–6 mm) are considered, an average limiting curve $c' = 0$ kPa, $\phi' = 20^\circ$ is obtained.

- (e) Several specimens were tested along planes inclined at 45° and 90° with respect to the horizontal. The results are collected in Fig. 42. No clear indication of anisotropy of the clay matrix was found, so it is possible that peak parameters determined for horizontal shearing may represent average peak strength.

Residual strength

Residual strength was investigated using two types of test: ring shear tests on remoulded specimens, and direct shear tests on natural discontinuities. Twelve ring shear tests were performed, on samples recovered in the first 20 m of clay, at normal stresses of either 200 kPa or 700 kPa. An average residual friction angle of 13° was measured. No changes with depth were found. The weathered brownish upper clay levels were also tested, and no differences in residual friction were observed.

Natural joints found on the large clay blocks deposited by the mudflow (Fig. 12) were tested in the shear box. The discontinuity was aligned with the shearing plane of the box. Several reversing cycles were applied, and displacements in excess of 60 mm were achieved. For vertical stresses in the range 200–400 kPa a friction angle $\phi'_{res} = 11^\circ$ was found (Fig. 43).

Synthesis of direct shear strength results

The results of all direct shear tests performed on horizontal planes are summarised in Fig. 44. The average peak strength is obtained for a shear displacement of 1 mm. The open symbols in the figure correspond to the strength measured immediately after the peak at essentially the same displacement. The curved strength envelope is a reasonable approximation to the measured values. A straight line is also fitted to the points. The important result is that the sudden loss of strength results in a destruction of the effective cohesion. An accumulation of shear displacements of 6 mm implies a drop of friction angle down to 18 – 20° . Finally, the residual friction envelope, associated with further additional displacements, is also plotted in the figure.

Unconfined compression and triaxial tests

Specimens recovered in boreholes S1-2, S3-1 and S4-1 were tested in unconfined compression. A moderate increase of strength with depth was found. A representative value of $q_u \cong 250$ – 300 kPa is found at the level of the basal failure plane. A well-defined rupture plane developed in all the tested specimens. Initial secant moduli in the range $E_u = 10$ – 30 MPa for relatively high vertical deformations (1–2%) were measured.

Several isotropically consolidated undrained tests were performed in a stress-path cell. Peak strengths correspond to friction angles in the range $\phi' = 31$ – 39° (Fig. 45). For the final conditions (vertical strains in excess of 20%), the friction angle drops to 15 – 21° . The maximum values of Skempton's A -coefficient ($A_{max} = 0.7; 0.45; 0.24; 0.49; 0.8$) reflect a moderate contractant behaviour before the onset of dilatancy. Near the peak some dilatancy develops, and the final A values indicate this change ($A_f = 0.6; 0.35; -0.03$;

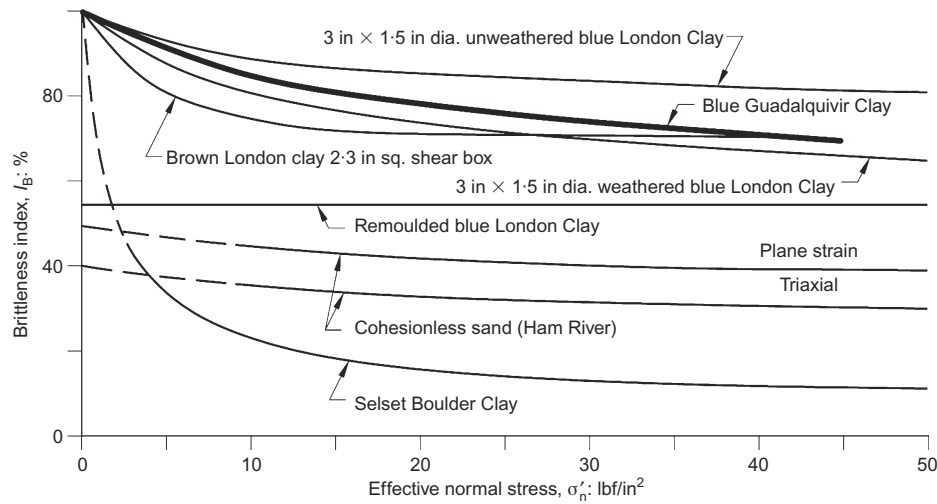
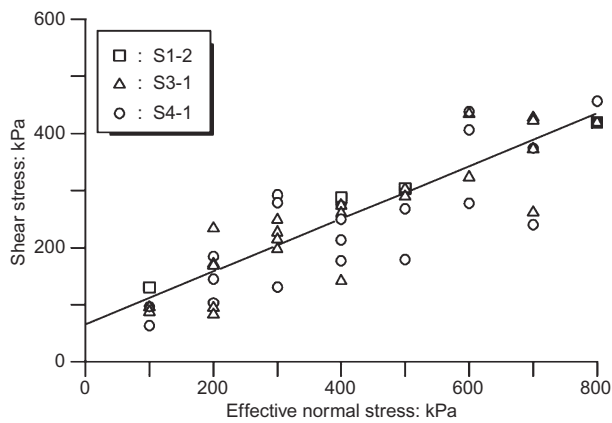

 Fig. 40. Comparison of brittleness index I_B with other values reported by Bishop *et al.* (1971)


Fig. 41. Drained peak strength envelope for Guadalquivir blue clay

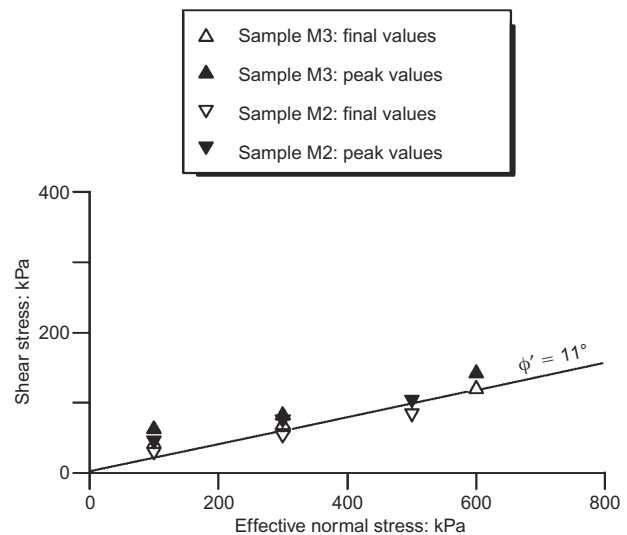


Fig. 43. Summary of direct shear tests performed on two natural discontinuities of the clay

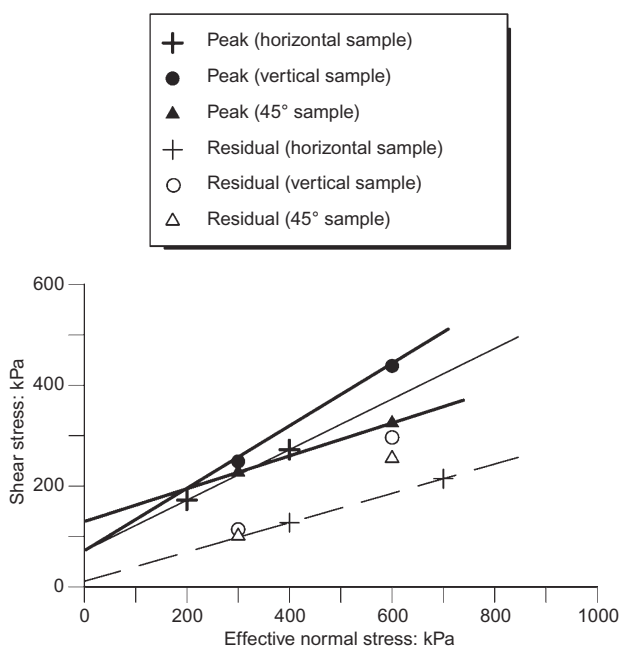


Fig. 42. Shear strength measured in inclined samples of foundation clay

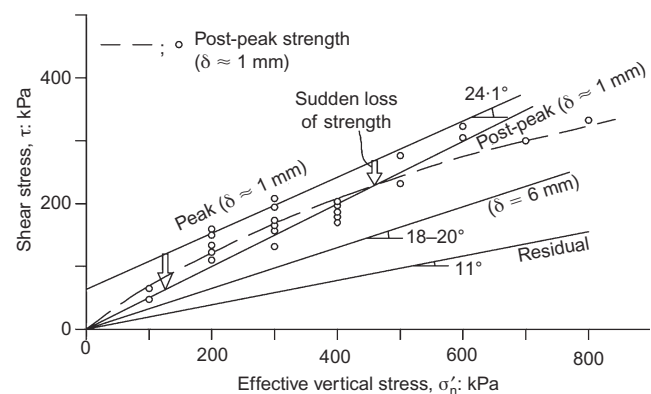


Fig. 44. Direct shear strength envelopes of foundation clay

0.20; 0.55). The 'elastic' value of $A = 0.33$ is probably a reasonable average value. Elastic moduli measured at relatively low strains ($\epsilon_z = < 2 \times 10^{-3}$) were in the range 55–115 MPa for confining stresses varying from 400 to 600 kPa.

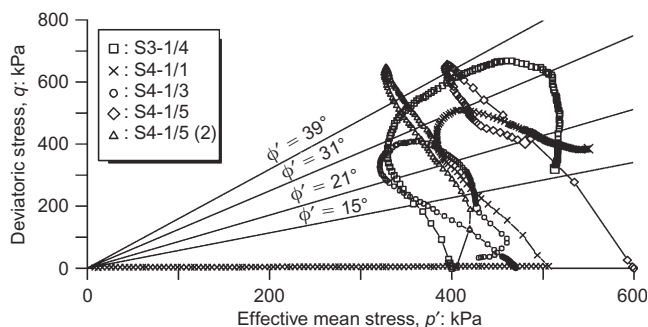


Fig. 45. Stress paths measured in isotropic undrained triaxial tests

Oedometer tests

The main objective of oedometer tests was to derive c_v values for the vertical stresses prevailing in the upper 20 m of the clay unit. Material parameters were derived from an automated back-analysis procedure of the measured deformation–time curves. The variation of values of c_v was small: $c_v = 0.5$ to 1.5×10^{-3} cm²/s (average: $c_v = 1 \times 10^{-3}$ cm²/s). Vertical permeability k was found to vary between 2 and 7×10^{-9} cm/s. No particular trends were detected in c_v or k over the upper 20 m of the clay formation.

A REVIEW OF THE FEATURES OF THE LANDSLIDE

The field observations and soil properties, when considered together, offer an improved understanding of the sliding failure, and these are reviewed in the context of the geotechnical properties.

The Aznalcóllar failure is an unusual case of deep translational sliding involving the entire dam, which displaced a large distance (50 m in the central part) as a rigid body and suffered only minor distortions.

The head of the slide may be properly described as a remarkable subvertical cliff, around 20–22 m in height, which developed at the upstream foot of the rockfill dam. The foundation clay has a distinct vertical jointing, often orientated in the N–S and NE–SW directions. This geometry facilitated the development of the vertical failure plane in the clay and the direction of the embankment opening, discussed in connection with Figs 17 and 21. The properties of the tailings, particularly the pyrite tailings in the southern pond, explain the considerable near-vertical height of the exposed tailings at the rear scarp. The low permeability (10^{-6} to 10^{-7} m/s) indicates that the initial unloading associated with the forward motion of the slide was essentially undrained.

A simple calculation shows that the measured unconfined strengths were able to explain the observed stability of tailings. The average undrained strength necessary to ensure stability of a vertical cut is $\tau_f = 0.25\gamma H$. For $\gamma = 32$ kN/m³ and $H = 20$ m, $\tau_f = 165$ kPa. This strength was probably available in the whole deposit, as the plot in Fig. 28 indicates. Safety conditions would be expected to worsen with time, but field observations indicated a good stability over time as the reduction of water level in the pond, after the failure, probably induced an additional beneficial effect of suction.

It is also interesting to note that the failure did not involve any shearing of the tailings or the rockfill. Both are materials with a high friction angle. Consequently, the stability was controlled by only one material: the highly plastic and brittle Guadalquivir clay. It is believed that the stability of the tailings considerably reduced the consequences of the failure, both in terms of the size of the embankment opening

(controlled by the displacement of the embankment) and in terms of the total volume of the spill.

Turning now to the clay foundation, it is clear that the clay had a strong potential for progressive failure, given its brittleness. In addition, the downstream construction of the embankment is a process that favours the development of this mechanism, as explained in more detail in the companion paper (Gens & Alonso, 2006).

The fact that the sliding plane followed a bedding plane is also an indication that the strength of the clay formation was not isotropic. The strength isotropy measured in direct shear tests refers only to the clay matrix. It is concluded that some initial ‘damage’ was probably present in the bedding planes. The striated surfaces discovered in some of the boreholes and outcrops also favour this interpretation. Therefore the reduced available initial strength along bedding planes and the mechanisms of progressive failure are two factors that probably contributed to a reduction of the available mean strength of the clay to resist the driving forces induced by dam and tailings.

The large quasi-horizontal displacement of the dam is another interesting feature of this failure, which has to be related to the evolution of driving and resisting forces, once the failure has initiated. The brittleness of the clay and the low residual friction angle indicate that, once the failure has initiated, there is a potential for an accelerated motion due to the progressive loss of clay strength.

The 1.5 km-long dam that bounds the eastern side of the lagoon had a constant height of around 27 m. In contrast, the western side is constituted of a small embankment sitting on top of a natural ground elevation. The northern and southern portions of the perimeter dam had, therefore, a very small height at the western corner and an increasing height as they approached the eastern side. A question raised during the investigation of the failure is why the failure affected only the southern portion of the east embankment and not the northern one. A proper explanation of this aspect is also required for a thorough understanding of the causes of the failure.

A number of circumstances help to explain why the sliding took place in the south-eastern part of the embankment and not in the northern one.

- The direction of thrust from the tailings was closer to the orientation of the dip of the bedding planes. This aspect will be examined in detail in the companion paper (Gens & Alonso, 2006).
- The southern lagoon stored pyrite tailings, which have a higher density than the pyroclast tailings stored in the northern lagoon.
- The level of tailings was somewhat higher in the southern lagoon. This was a consequence of the procedure for placing the tailings in the lagoon. The most recent placement was made from an outlet located in the southern lagoon, at the corner formed by the central jetty and the eastern embankment.
- The river bed of the Agrio river was closer to the embankment downstream toe at this location owing to a meander (Figs 1 and 6). (A quantification of the effect of this meander by means of limit equilibrium methods indicated, however, that it had only a marginal effect on safety.)

The displacement of the embankment decreased towards the south because of a stabilising berm placed against the rock-fill embankment, at the southern end of the embankment. ‘Corner’ conditions also contributed to a reduction of the sliding risk. In the northern part of the slide two circumstances favoured the stability of the embankment: its overall width is 20 m greater than the width of the failed embank-

ment, and the orientation of the embankment changes 20° towards the north-west.

This paper has provided field information and laboratory results related to the Aznalcóllar dam failure. A description of the slide has been given, but an understanding of the reasons for the failure requires the performance of stability analyses, as presented in a companion paper (Gens & Alonso, 2006).

ACKNOWLEDGEMENTS

The authors wish to thank Professor A. Lloret and Dr J. Moya for their contribution during the performance of the work described in this paper.

NOTATION

A	activity; Skempton's pore pressure coefficient
A_f	A value near peak conditions in undrained triaxial tests
A_{\max}	maximum A value
C_u	coefficient of uniformity
c'	effective cohesion
c_v	coefficient of consolidation
CL_f	$(= \Delta\tau_b/(\tau_p - \tau_f))$ cementation loss index (with respect to 'end of test' conditions)
CL_B	$(= \Delta\tau_b/(\tau_p - \tau_{\text{res}}))$ cementation loss index (with respect to residual conditions)
\overline{CL}_f	average of CL_f among tests performed
\overline{CL}_B	average of CL_B among tests performed
d_p	displacement at peak strength in direct shear tests
e	void ratio
E_m	constrained modulus in oedometer tests
E_u	secant undrained modulus
I_f	$(= (\tau_p - \tau_f)/\tau_p)$ brittleness index (with respect to 'end of test' conditions)
I_B	$(= (\tau_p - \tau_{\text{res}})/\tau_p)$ brittleness index (with respect to residual conditions)
I_p	plasticity index
p'	effective mean stress, $(\sigma'_1 + 2\sigma'_3)/3$.
q'_f	deviatoric shear stress at failure $(\sigma'_1 - \sigma'_3)$ (at maximum pore pressure if triaxial tests on tailings)
w_L	liquid limit
α	angle of orientation of specimens with respect to the vertical
γ_s	unit weight of solids
γ_{sat}	saturated unit weight
γ_w	unit weight of water
δ	horizontal displacement in direct shear tests
σ'_{initial}	effective mean confining stress (in triaxial tests on tailings).
σ'_n, σ'_v	normal or vertical effective stress

$\tau_f, \tau_{\text{final}}$	shear strength measured at maximum displacement in direct shear tests
τ_p	peak shear strength in direct shear tests
τ_{res}	residual shear strength
$\Delta\tau_b$	sudden drop of shear strength after peak in direct shear tests
ϕ'	effective friction angle
ϕ'_{res}	effective residual friction angle

REFERENCES

- Alonso, E., Gens, A. & Lloret, A. (1992). The landslide of Cortes de Pallás, Spain: a case study. *Géotechnique* **42**, No. 4, 601–624.
- Bishop, A. W. (1967). Progressive failure: with special reference to the mechanism causing it. *Proceedings of the geotechnical conference on shear strength properties of natural soils and rock*, Oslo, Vol. 2, pp. 142–150.
- Bishop, A. W., Green, G. E., Garga, V. K., Andresen, A. & Brown, J. D. (1971). A new ring shear apparatus and its application to the measurement of residual strength. *Géotechnique* **21**, No. 4, 273–328.
- Burland, J. B., Longworth, T. I. & Moore, J. F. A. (1977). A study of ground movement and progressive failure caused by a deep excavation in Oxford clay. *Géotechnique* **27**, No. 4, 557–591.
- Chandler, R. J., Willis, M. R., Hamilton, P. S. & Andreou, I. (1998). Tectonic shear zones in the London Clay Formation. *Géotechnique* **48**, No. 2, 257–270.
- Gens, A. & Alonso, E. E. (2006). Aznalcóllar dam failure. Part 2: Stability conditions and failure mechanism. *Géotechnique* **56**, No. 3, 185–201.
- Olalla, C. & Cuéllar, V. (2001). Failure mechanism of the Aznalcóllar Dam, Seville, Spain. *Géotechnique* **51**, No. 5, 399–406.
- Petley, D. J. (1984). Shear strength of over-consolidated fissured clay. *Proc. 4th Int. Symp. on Landslides, Toronto* **2**, 167–172.
- Rodríguez Vidal, J. (1989). La evolución neotectónica del sector occidental de la depresión del Guadalquivir. El Cuaternario en Andalucía Occidental. *AEQUA Monografías*, **1**, 21–26.
- Rodríguez Vidal, J. & Flores Hurtado, E. (1991). Evidencias de deformación neotectónica en el sector de Lepe-La Antilla (Huelva). *Cuaternario y Geomorfología* **5**, 131–138.
- Skempton, A. W. & Petley, D. J. (1967). The strength along structural discontinuities in stiff clays. *Proceedings of the geotechnical conference on shear strength properties of natural soils and rock*, Oslo, Vol. 2, pp. 29–46.
- Skempton, A. W., Schuster, R. L. & Petley, D. J. (1969). Joints and fissures in the London clay at Wraysbury and Edgware. *Géotechnique* **19**, No. 2, 205–217.
- Tsige, M. (1998). *Microfábrica y mineralogía de las arcillas azules del Guadalquivir: influencia en su comportamiento geotécnico*. PhD thesis, Departamento de Geodinámica, Facultad de Ciencias Geológicas, Universidad Complutense de Madrid.